Macromolecules

Article

Cite This: Macromolecules 2019, 52, 8374−8383

pubs.acs.org/Macromolecules

Competing Hydrogen Bonding Interaction Creates Hierarchically Ordered Self-Assembled Structures of PMMA-*b*-P4VP/PVPh-*b*-PS Mixtures

Cheng-Tai Tsou and Shiao-Wei Kuo*

Department of Materials and Optoelectronic Science, Center of Crystal Research, National Sun Yat-Sen University, Kaohsiung 80424, Taiwan

Supporting Information

ABSTRACT: In this study, poly(methyl methacrylate-*b*-4-vinylpyridine) (PMMA-*b*-P4VP) and poly(vinylphenol-*b*-styrene) (PVPh-*b*-PS) block copolymers were synthesized through anionic living polymerization; together, they featured one hydrogen bonded donor segment (PVPh) and two hydrogen bonded acceptors (PMMA and P4VP). Initially we investigated diblock copolymer/homopolymer blends of PMMA-*b*-P4VP/PVPh blends, where PVPh homopolymer (C) could act as the common solvent for PMMA-*b*-P4VP (A-*b*-B) copolymer. Short range ordered of self-assembled structure formed for pure PMMA-*b*-P4VP copolymer and for its blends with PVPh at lower concentrations; at higher PVPh concentrations, however, miscible disordered structures formed because of OH units of PVPh both interacted with P4VP and PMMA segments. In addition, blending the immiscible PMMA-*b*-P4VP into the PVPh-*b*-PS diblock copolymer resulted in full morphological transitions: from the lamellae, double gyroid, cylinder, sphere, and, finally, to disordered structures. Therefore, the ΔK effects for competitive hydrogen bonding among PVPh/PMMA and PVPh/P4VP binary pairs, these PMMA-*b*-P4VP/PVPh-*b*-PS blends exhibited several hierarchical nanostructures, including core/shell (coaxial) cylinder, cylinder-in-lamellae, and core/shell double-gyroid structures.

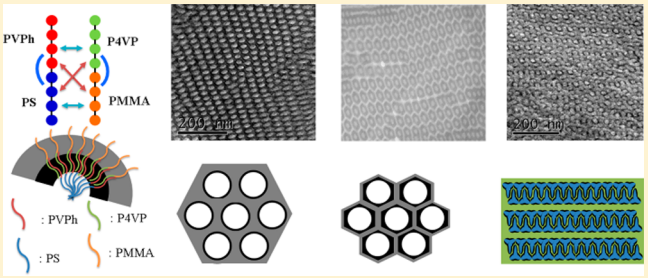

INTRODUCTION

Self-assembly nanostructures from immiscible diblock copolymers (A-*b*-B) including alternative lamellar, double-gyroid, hexagonal packed cylinder, and spherical structures have potential applications in nanocomposites, photonic crystals, and nanomedicines.[1−5] Because the volume fraction or degree of polymerization of each block segment can be difficult to control through living polymerization, blending of a homopolymer C capable of noncovalent bonding (e.g., electrostatic, ionic, or hydrogen bonding interactions) into the A-*b*-B diblock copolymer is a relative simpler approach for mediating the volume fraction of each block copolymer segment.[6−10] In previous theoretical and experimental studies, we have investigated the behavior of four different A-*b*-B/C blends mediated through hydrogen bonding interaction.[11−29] We observed two-phase systems [Scheme 1a] for these A-*b*-B/C blends, with the nature of the self-assembly nanostructures typically formed—lamellar, cylinder, spherical, or even double-gyroid morphologies—strongly dependent on the relative hydrogen bonding strength between hydrogen bond donors and acceptors of each block segment.[15−17] For example, PVPh-*b*-PS exhibited dry-brush or disordered self-assembled structures when blended with the PMMA homopolymer, with which it interacted weakly through hydrogen bonding; in contrast, it exhibited wet-brush behavior with a full order−order transition as blending with the P4VP homopolymer, with which it experiences strong hydrogen bonding.[15,16] These phenomena are directly related to the hydrogen bonding strengths. The interassociation equilibrium constants (K_A) in PVPh/PMMA and PVPh/P4VP are 37.4 and 1200, respectively, while the self-association equilibrium constant (K_B) of PVPh is 66.8; thus, the ratio K_A/K_B could act as the factor determining the type of self-assembly nanostructure from such A-*b*-B/C blend, and it can also be predicted theoretically using the attractive interaction model (AIM).[17]

In addition to AB diblock copolymer, more complex ABC triblock copolymer have received much attention because they also form various hierarchical nanostructures, including core/shell (coaxial) cylinder, three-phase lamellae, cylinder-in-lamellae, core/shell double-gyroid, and other complicated nanostructures.[30,31] As an alternative to the potentially difficult and complicated syntheses of ABC triblock copolymers, the blending of AB and CD diblock copolymer with hydrogen bonding is the relatively simpler approach for preparing such hierarchical nanostructures. Three different systems have been developed for these AB/CD mixtures stabilized through hydrogen bonding.[32−40] The first, proposed by Matsushita et al., featured immiscible PS-*b*-PVPh (AB) blended with

Received: September 2, 2019
Revised: October 20, 2019
Published: October 29, 2019

DOI: 10.1021/acs.macromol.9b01829
Macromolecules 2019, 52, 8374−8383

Scheme 1. Cartoon Representations of the Transformations of System Experiencing Specific Interactions: (a) A-*b*-B + C Becoming a Two-Phase System (2 Phases + 1 Phase Becoming 2 Phases), (b–d) A-*b*-B + C-*b*-D for (b) Becoming a Three-Phase System (2 Phases + 2 Phases Becoming 3 Phases), (c) Becoming a Three-Phase System (2 Phases + 1 Phases Becoming 3 Phases), and (d) Becoming a Two-Phase System (1 Phases + 1 Phases Becoming 2 Phases)

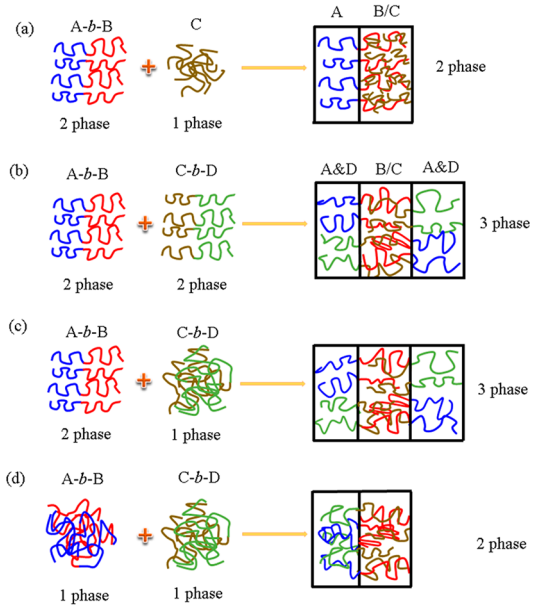

immiscible poly(2-vinylpyridine–*b*–isoprene) (P2VP-*b*-PI, CD), with a miscible PVPh/P2VP (B/C) domain (featuring strong hydrogen bonding) and immiscible PS (A) and PI (D) block segments; these systems formed a lamellar-within-lamellar structure as a three-phase system (2 + 2 phase becomes 3 phase), as shown in Scheme 1(b).[34] We developed the second system by blending immiscible PS-*b*-P4VP (AB) with miscible disordered PVPh-*b*-PMMA (CD), giving a so-called "2 + 1 phase becomes 3 phase" system, where the PMMA block domain (D) was excluded from the miscible PVPh-*b*-PMMA through the introduction of strong hydrogen bonding for miscible PVPh/P4VP (B/C) domain, resulting in immiscible PS (A) and PMMA (D) block segments.[38] A similar system formed as blending immiscible PS-*b*-PVPh with miscible disordered P4VP-*b*-PEO, leading to one miscible PVPh/P4VP (B/C) domain as well as immiscible PS (A) and PEO (D) block segments, resulting in core/shell (coaxial) cylindrical or three-phase lamellar structures [Scheme 1c].[39] We also developed the third system from two miscible disordered P4VP-*b*-PEO and PMMA-*b*-PVPh mixtures, which formed one miscible PVPh/P4VP (B/C) domain and another miscible PMMA/PEO domain, giving a so-called "1 + 1 phase becomes 2 phases" structure, as depicted in Scheme 1d.[40]

In this present study, we combined the concepts in Scheme 1a,b to investigate the self-assembly nanostructures from related diblock copolymer mixtures. As mentioned above, the self-assembly structures for A-*b*-B/C blends are dependent on the relative hydrogen bonding strength: for example, PVPh-*b*-PS blended with the P4VP homopolymer exhibits wet-brush behavior with strong hydrogen bonding, whereas it displays dry-brush behavior when blended with the PMMA homopolymer with weak hydrogen bonding.[15] Therefore, we were interested in covalently linking these homopolymers into a PMMA-*b*-P4VP and blending it with PVPh-*b*-PS to form potentially interesting related self-assembled nanostructures. Furthermore, in the "2 + 2 phase becomes 3 phase" system in Scheme 1b, PVPh segment usually interacts only with the P2VP or P4VP block segment, and not with the A or D block segment (e.g., PS or PI). As a result, we suspected that related hierarchical nanostructures—including core/shell cylinder, cylinder-in-lamellae, and core/shell double-gyroid structures—would form from PMMA-*b*-P4VP/PVPh-*b*-PS blends where PVPh block could both interact with P4VP and PMMA segments by hydrogen bonding. Herein, we report the results of such studies, along with corresponding examinations of the miscibility behavior and competitive hydrogen bonding.

MATERIALS

Styrene, 4-*tert*-butoxystyrene, 4-vinylpyridine, and methyl methacrylate were purchased from Aldrich. *sec*-Butyllithium (1.3 M in cyclohexane) was obtained from Acros. Diblock copolymer of $PVPh_{129}$-*b*-PS_{100} was prepared by anionic living polymerization

Scheme 2. Synthesis of the Diblock Copolymers (a) PMMA-*b*-P4VP and (b) PVPh-*b*-PS by Sequential Anionic Living Polymerization

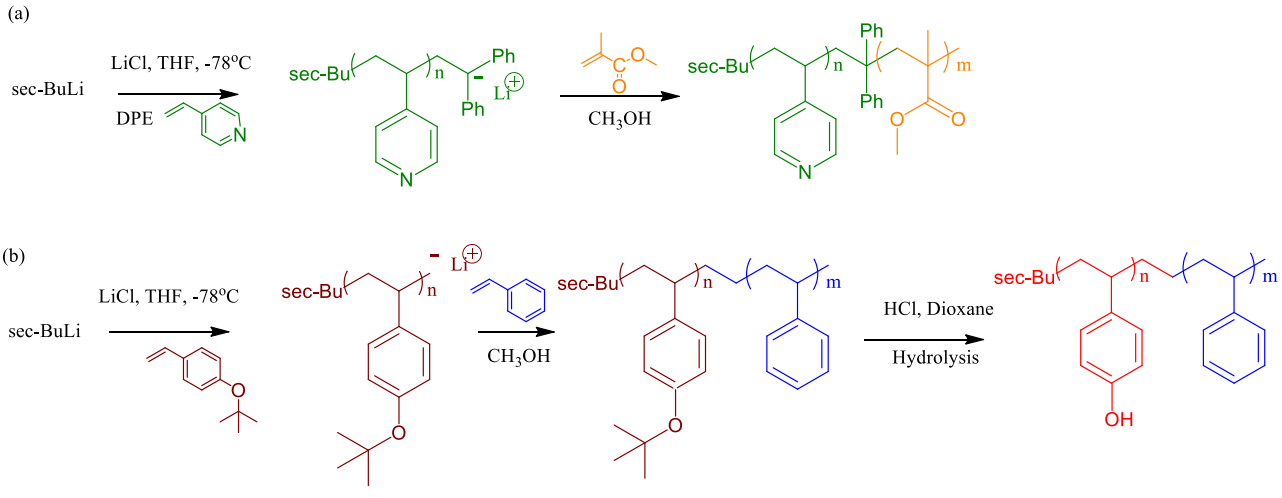

DOI: 10.1021/acs.macromol.9b01829
Macromolecules 2019, 52, 8374–8383

Table 1. Molecular Weights, Molar Volumes, Solubility Parameters, Values of K_A and K_B, and Scattering Length Densities of Each Block Segment in This Tested Diblock Copolymer Blends

	molecular weight	molar volume	solubility parameter	equilibrium constants			scattering length density
block	(g/mol)	(mL/mol)	$(cal/mL)^{1/2}$	K_2	K_B	K_A	$(10^{-6}/Å^2)$
PMMA	100.0	84.9	9.1			37.4	10.841
P4VP	105.1	84.9	10.8			1200	10.063
PVPh	120.1	82.3	11.0	21.0	66.8		10.520
PS	104.1	93.9	9.5				9.516

[a]Self-association equilibrium constants: K_2 (dimer) and K_B (multimer); interassociation equilibrium constant: K_A.

while using the *tert*-butyloxy group as a protective unit for poly(4-*tert*-butoxyystyrene-*b*-styrene) (P*t*BOSS-*b*-PS), as displayed in Scheme 2a; this approach is discussed in detail elsewhere.[41] $PMMA_{38}$-*b*-$P4VP_{160}$ was also synthesized by anionic living polymerization, with the addition of MeOH terminating the polymerization, as displayed in Scheme 2b; the degrees of polymerization of the PVPh and P4VP segments were similar.[42,43] The $PVPh_{130}$ homopolymer was prepared through anionic polymerization.

PMMA-*b*-P4VP/PVPh-*b*-PS Blends. The PMMA-*b*-P4VP/PVPh-*b*-PS blends were prepared by the solution-blending. Mixtures (10 wt %) of the diblock copolymers were prepared by dissolving in DMF, which was the common solvent for each block segment. Each diblock copolymer mixture was stirred overnight at 40 °C and then cast on a Teflon disk. DMF was evaporated at 80 °C for 3 days, and then the sample was dried under a vacuum at 100 °C over 1 week.

RESULTS AND DISCUSSION

Synthesis of PMMA-*b*-P4VP and PVPh-*b*-PS Diblock Copolymers. We synthesized PMMA-*b*-P4VP by sequential anionic living polymerization, as presented in Scheme 2(a). FTIR spectrum of the PMMA-*b*-P4VP featured [Figure S1(a)] the C = O absorption at 1731 cm^{-1} (from the PMMA segment) as well as signals for the pyridyl units at 1598 and 993 cm^{-1} (from the P4VP segment). Its ^1H NMR spectrum [Figure S1(b)] featured a signal for the O−CH_3(peak g) group of the PMMA segment at 3.56 ppm and signals for the pyridyl units of the P4VP segment at 6.56 and 8.22 ppm. The molar ratio of the P4VP segment was much higher than that of the PMMA segment, based on ^1H NMR spectral analysis; the molecular weight of $PMMA_{38}$-*b*-$P4VP_{160}$ (PDI = 1.09) was determined through SEC analysis. The synthesis of PVPh-*b*-PS through sequential anionic polymerization has been applied widely, with a *tert*-butyl group used as a protective unit, as displayed in Scheme 2b.[41−43] We used the polymerization of the PVPh homopolymer as a model reaction, with phenolic OH groups observed (based on FTIR and NMR spectroscopic analyses) after total removal of *tert*-butyl units (Figure S2). The broad absorption appeared at 3340 cm^{-1}, representing the OH units, after hydrolysis, as displayed in Figure S2(A)-(b). Furthermore, the signal at ca. 1.30 ppm [Figure S2(B)-(c)] representing the *tert*-butyl units disappeared after the deprotection, with a new signal appearing at 8.93 ppm, representing the OH groups of PVPh homopolymer, as displayed in Figure S2(B)-(d). The spectra of the PVPh-*b*-PS diblock copolymer displayed features similar to those of the PVPh homopolymer, as presented in Figure S3; the molecular weight of $PVPh_{129}$-*b*-PS_{100} (PDI = 1.05) was determined through SEC.

Self-Assembled Structures of PMMA-b-P4VP/PVPh Blends. Table 1, Scheme 1b, and Scheme S1 summarize the physical properties for PMMA-*b*-P4VP/PVPh-*b*-PS blends. Six different interaction parameters of AB/CD blends could be expected (Scheme S1): two of them are negative, namely those for the PVPh/PMMA and PVPh/P4VP binary pairs, indicating these two blend systems have disordered structures or are miscible blend systems, while the other four are positive, namely those for the PVPh/PS, P4VP/PS, P4VP/PMMA, and PS/PMMA blends, which are either phase-separated or immiscible blend systems. This system possessed an additional miscible binary pair relative to the PI-*b*-P4VP/PVPh-*b*-PS system,[34] which exhibited only one miscible binary pair (the miscible PVPh/P4VP domain). Furthermore, the K_A value of the PVPh/P4VP (1200) was much higher than the PVPh/PMMA blend (37.4), implying that PVPh prefers to interact with the P4VP block, rather than the PMMA block, through hydrogen bonding.

Following on from our earlier studies of the self-assembled nanostructures formed when blending PVPh-*b*-PS with P4VP or PMMA homopolymer (wet-brush behavior with a full order−order transition upon blending with P4VP with strong hydrogen bonding; dry-brush or disordered structure upon blending with PMMA with weak hydrogen bonding),[15] we began our investigation of the miscibility and self-assembly structures of PMMA-*b*-P4VP/PVPh blend for comparison with that of PMMA-*b*-P4VP/PVPh-*b*-PS blends. Figure 1A presents

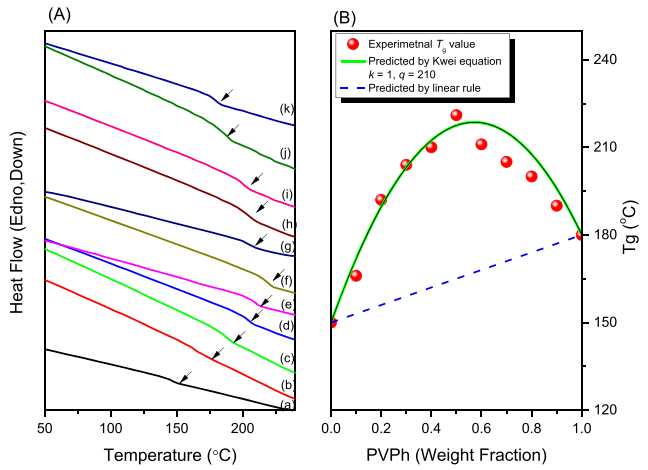

Figure 1. (A) DSC thermograms of PMMA-*b*-P4VP/PVPh blends: (a) 100/0, (b) 90/10, (c) 80/20, (d) 70/30, (e) 60/40, (f) 50/50, (g) 40/60, (h) 30/70, (i) 20/80, (j) 10/90, and (k) 0/100. (B) Glass transition temperatures of the miscible P4VP/PVPh domains of the PMMA-*b*-P4VP/PVPh blends.

the second heating scans of the DSC analyses for PMMA-*b*-P4VP/PVPh blends. Our pure PMMA-*b*-P4VP displayed a glass transition temperature (T_g) near 150 °C for the P4VP segment; we did not observe glass transition behavior for the PMMA segment, presumably because its degree of polymerization was lower than that of the P4VP segment in this diblock copolymer. Furthermore, we also observed a T_g value

DOI: 10.1021/acs.macromol.9b01829
Macromolecules 2019, 52, 8374−8383

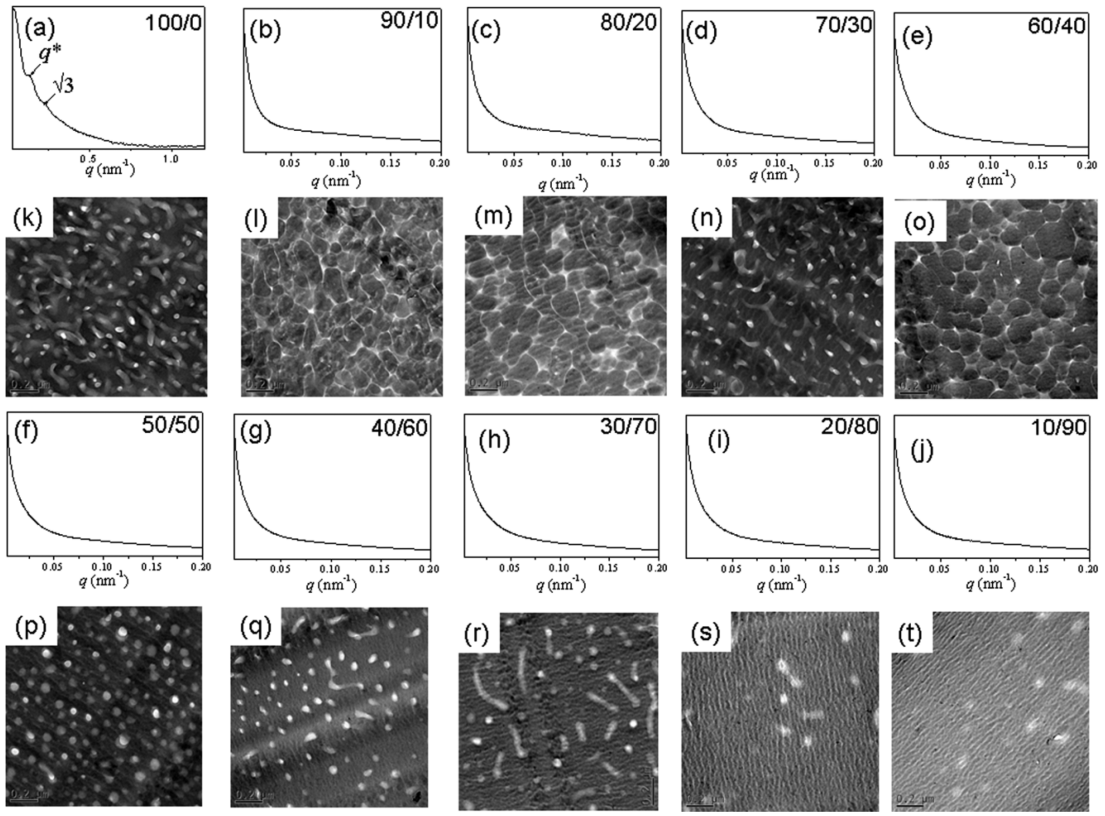

Figure 2. (a–j) SAXS and (k–t) TEM analyses for the PMMA-*b*-P4VP/PVPh blends (a, k) 100/0, (b, l) 90/10, (c, m) 80/20, (d, n) 70/30, (e, o) 60/40, (f, p) 50/50, (g, q) 40/60, (h, r) 70/30, (i, s) 80/20, and (j, t) 90/10.

of approximately 180 °C for our PVPh homopolymer. The T_g value for P4VP segment increased significantly after blending with the PVPh homopolymer, due to strong intermolecular hydrogen bonding in PVPh/P4VP domain. The highest value of T_g was approximately 221 °C for the PMMA-*b*-P4VP/PVPh = 50/50 blend; this value is much higher than that of the homopolymer blend P4VP/PVPh = 50/50 (T_g = 190 °C) prepared from DMF solution, presumably due to the nanoconfinement effect from diblock copolymer. Figure 1B displays the behavior of the values of T_g for PVPh/P4VP domain in PMMA-*b*-P4VP/PVPh blends. The glass transition temperatures for miscible PVPh/P4VP complex domains deviated positively from the linear equation; the Kwei equation can usually predict such values for strongly hydrogen bonding systems:[44]

$$T_g = \frac{W_1 T_{g1} + kW_2 T_{g2}}{W_1 + kW_2} + qW_1W_2 \quad (1)$$

where W_1 and W_2 are the weight fractions and T_{g1} and T_{g2} are the glass transition temperatures for PVPh and P4VP segments, respectively, while k and q are the corresponding fitting constants. Using a fitting procedure, we obtained a value of k of 1 and a value of q of 210, implying that this blend was a strongly hydrogen bonding system. Notably, this value of q was much higher than that of homopolymer blend for PVPh/P4VP system (q = 100).[45]

Figure 2 displays small-angle X-ray scattering (SAXS) and transmission electron microscopy (TEM) analyses of PMMA-*b*-P4VP/PVPh blends at various PVPh homopolymer concentrations. Pure PMMA-*b*-P4VP exhibited the short-range order of the cylinder structure [Figure 2a], based on a scattering peak ratio of 1:$\sqrt{3}$, which is confirmed by TEM analysis [Figure 2k]. This self-assembled nanostructure was destroyed upon blending with the PVPh homopolymer, with only a broad peak observed for all PMMA-*b*-P4VP/PVPh blend compositions, as displayed in Figure 2b–j. Nevertheless, the TEM images of the samples obtained with PVPh concentrations of less than 70 wt % displayed [Figure 2l–r] the short-range order of wormlike or micelle structures. The broad SAXS patterns may have correlated with electron density differences that were not sufficiently high to observe the q reflections at these compositions. As PVPh concentration was higher than 80 wt %, the miscible disordered structures were observed [Figure 2s,t]. This result is consistent with previous studies of immiscible A-B diblock copolymers, where the C homopolymer is both miscible with the A and B blocks. For example, many reports of PCL-*b*-P2VP, PCL-*b*-P4VP, or PMMA-*b*-P2VP blends with PVPh have revealed that the self-assembled nanostructures vary from ordered structures to miscible disordered structures, dependent on the degree of the ΔK effect.[18−25] This ΔK effect is because of the different hydrogen bonding strengths of the B/C units (e.g., K_A = 1200 for PVPh/P4VP blends) compared with the A/C units (e.g., K_C = 37.4 for PVPh/PMMA blends; K_C = 90 for PVPh/PCL blends).[46]

Figure 3 displays FTIR spectra of the PMMA-*b*-P4VP/PVPh blends at various compositions, presenting the regions for the vibrations of the C = O units for PMMA segment [Figure 3a] and the pyridyl units for P4VP segment [Figure 3b]. As noted in Figure S1(a), the pure PMMA-*b*-P4VP diblock copolymer exhibited signals at 1731 cm^{-1} for free C = O units for PMMA block and at 993 cm^{-1} for free P4VP pyridyl unit. When blended with the PVPh homopolymer at concentrations greater than 80 wt %, the new signal was appeared at 1705

DOI: 10.1021/acs.macromol.9b01829
Macromolecules 2019, 52, 8374−8383

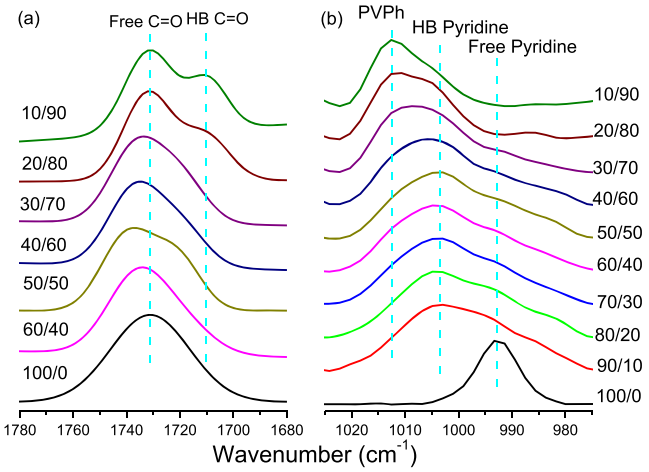

Figure 3. FTIR spectral analyses of PMMA-*b*-P4VP/PVPh mixtures: (a) C═O and (b) pyridyl vibrations.

cm^{-1}, as displayed in Figure 3a, corresponding to hydrogen-bonded PMMA C = O groups, while another new signal appeared at 1005 cm^{-1}, corresponding to the hydrogen-bonded P4VP pyridyl units, as displayed in Figure 3b. Both of these signals were fitted well using Gaussian functions; notably, to calculate the area fraction for hydrogen-bonded pyridyl units, we had to digitally subtract the signal from the PVPh homopolymer at 1013 cm^{-1}.[45]

Figure 4 summarizes the area fractions for hydrogen-bonded pyridyl and C═O units for the PMMA-*b*-P4VP/PVPh blends;

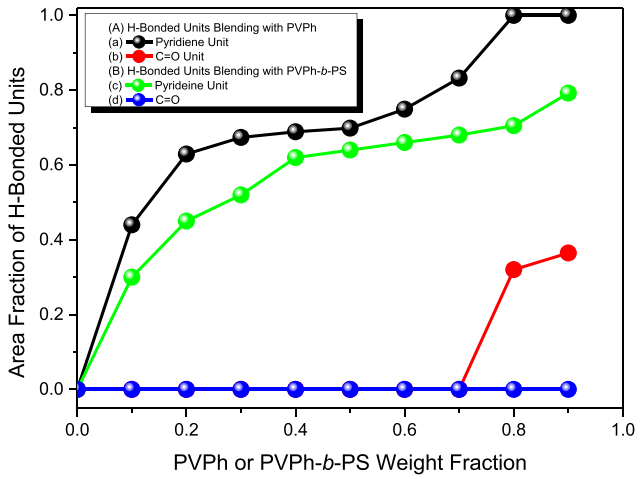

Figure 4. Area fractions of hydrogen-bonded (a, c) pyridyl and (b, d) C═O groups of (A) PMMA-*b*-P4VP/PVPh and (B) PMMA-*b*-P4VP/PVPh-*b*-PS blends.

both values were increased with the increase of PVPh concentration. At lower PVPh concentrations (<70 wt %), we did not observe any area fraction for PMMA C═O groups, because all of the PVPh OH units interacted with the P4VP pyridyl units—a result of K_A value for PVPh/P4VP being much higher than the PVPh/PMMA blend system. When the PVPh concentration was higher than 80 wt %, the area fraction of the hydrogen-bonded pyridyl units was close to 100%, such that free PVPh OH groups could also interact with the PMMA C═O groups through hydrogen bonding. As a result, as the PVPh concentration was higher than 80 wt %, the short-range-ordered self-assembled structure transformed into miscible disordered structures, as revealed using TEM images [Figure 2s,t], because the PVPh OH groups both interacted with P4VP and PMMA segments by hydrogen bonding, such that the PVPh homopolymer could act as the common solvent for PMMA-*b*-P4VP [24]. We conclude that, for this PMMA-*b*-P4VP/PVPh blend, short-range ordered of self-assembly nanostructures formed at lower PVPh concentrations, and they became miscible disordered structures at higher PVPh concentrations because the PVPh homopolymer (C) was the common solvent for both the PMMA (A) and P4VP (B) segments.

Self-Assembled Structures of PMMA-b-P4VP/PVPh-b-PS Blends. We expected to obtain six different interaction parameters for these PMMA-*b*-P4VP/PVPh-*b*-PS blends, as well as three types of phase behavior for the PMMA, PVPh/P4VP, and PS domains. Figure 5A presents the second heating

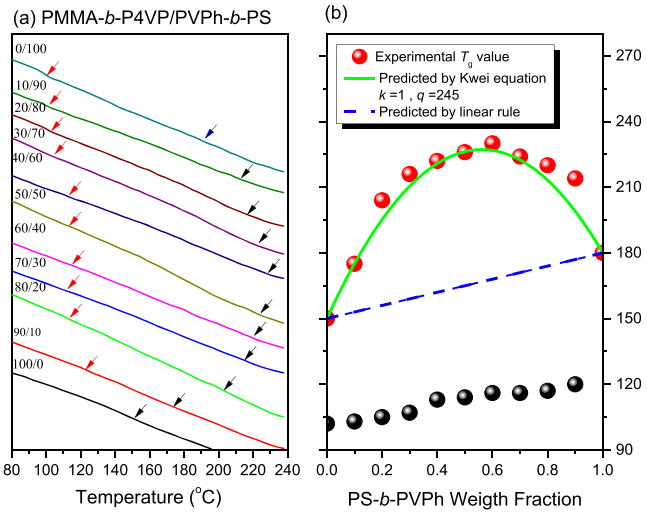

Figure 5. (a) DSC thermograms of PMMA-*b*-P4VP/PVPh-*b*-PS. (b) Glass transition temperatures of the miscible P4VP/PVPh domain of PMMA-*b*-P4VP/PVPh-*b*-PS blends.

thermograms in the DSC analyses for PMMA-*b*-P4VP/PVPh-*b*-PS blends. Pure PMMA-*b*-P4VP displayed a glass transition temperature of approximately 150 °C for the P4VP segment, as mentioned earlier. Pure PVPh-*b*-PS exhibited two values of T_g: at 180 °C for the PVPh domain and at 100 °C for the PS domain, implying that the PVPh and PS segments were microphase-separated. All of DSC thermograms of PMMA-*b*-P4VP/PVPh-*b*-PS featured two values of T_g. The higher of these values are corresponded to the miscible PVPh/P4VP domains; these values were much higher than those of the individual block segments, because of strong hydrogen bonding. The lower values of T_g corresponded to the PS segments, because the glass transition of the PMMA segment was not observed in DSC traces of PMMA-*b*-P4VP. Figure 5B also displays the T_g behavior for PVPh/P4VP domain and PS block segment for the PMMA-*b*-P4VP/PVPh-*b*-PS blends. Notably, the value of T_g of PS block increased upon increasing the PMMA-*b*-P4VP composition, because of the hard nanoconfinement effect of the high value of T_g from the miscible PVPh/P4VP domain. Furthermore, the highest value of T_g was located near 230 °C for the PMMA-*b*-P4VP/PVPh-*b*-PS = 40/60 blend system; this value is much higher than that of PMMA-*b*-P4VP/PVPh = 50/50 (T_g = 221 °C). As a result,

DOI: 10.1021/acs.macromol.9b01829
Macromolecules 2019, 52, 8374−8383

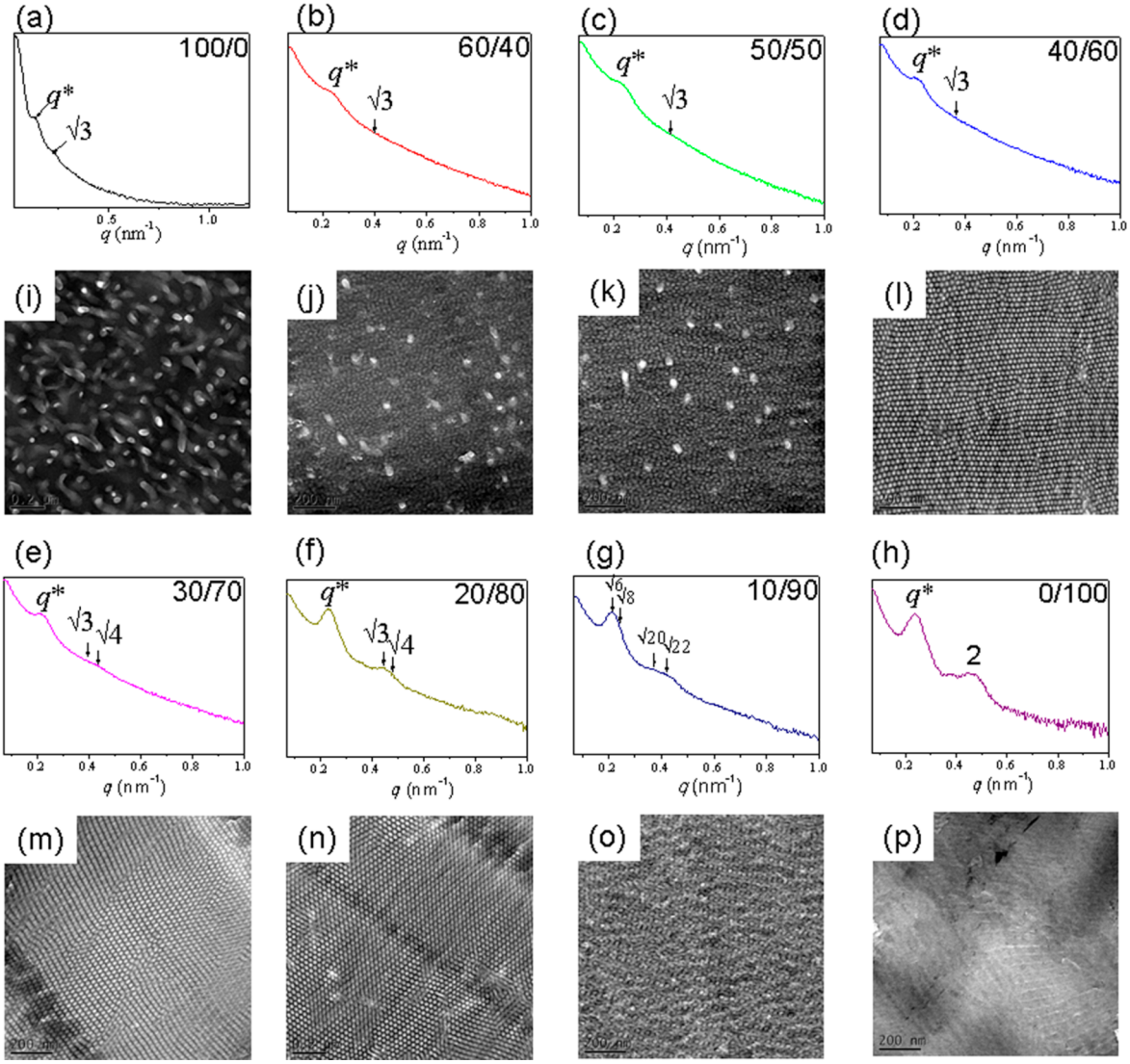

Figure 6. (a–h) SAXS patterns and (i–p) TEM images of the PMMA-*b*-P4VP/PVPh-*b*-PS blends (a, i) 100/0 (cylinder), (b, j) 60/40 (spherical micelle), (c, k) 50/50 (spherical micelle), (d, l) 40/60 (cylinder), (e, m) 30/70 (cylinder), (f, n) 20/80 (cylinder), (g, o) 10/90 (double-gyroid), and (h, p) 0/100 (lamellae).

we obtained a value of k of 1 and a value of q of 245, indicating a strongly hydrogen bonding system; this q value was higher than the PVPh/P4VP and PMMA-*b*-P4VP/PVPh mixtures, presumably due to the additional hierarchal nanoconfinement of both PS and PMMA blocks Nevertheless, the three-microphase behavior for this PMMA-*b*-P4VP/PVPh-*b*-PS blend was difficult to distinguish from the DSC thermograms.

Figure 6 presents SAXS and TEM images for PMMA-*b*-P4VP/PVPh-*b*-PS blends containing various contents of PVPh-*b*-PS. The SAXS pattern for pure PMMA-*b*-P4VP [Figure 6a] exhibited the short-range order of the cylinder structure, the same as that in Figure 2a, based on a scattering peak ratio of $1:\sqrt{3}$, consistent with the TEM analysis (Figure 6i); the first peak in the SAXS pattern appeared at a value of q^* of 0.137 nm^{-1} (d = 45.83 nm). Furthermore, pure PVPh-*b*-PS diblock copolymer possessed a lamellar structure, as displayed in Figure 6h, based on a scattering peak ratio of 1:2, which is confirmed by TEM [Figure 6p]; the first peak appeared in the SAXS pattern at a value of q^* of 0.241 nm^{-1} (d = 26.05 nm) and the PS volume fraction was approximately 0.47 in this block copolymer. For the sample PMMA-*b*-P4VP/PVPh-*b*-PS = 10/90, the TEM image [Figure 6o] revealed the long-range order of a double-gyroid structure from the [211] direction, as confirmed through SAXS analysis [Figure 6g] with a peak ratio of $\sqrt{6}:\sqrt{8}:\sqrt{20}:\sqrt{22}$. This interesting order–order transition from lamellae to double-gyroid structures has been observed previously for PVPh-*b*-PS/P4VP blends in which the PS volume fraction was 0.41–0.48.[15] In the sample PMMA-*b*-P4VP/PVPh-*b*-PS = 10/90, the PS volume fraction was approximately 0.43, consistent with those previous findings. When the PMMA-*b*-P4VP concentrations were 20, 30, and 40 wt %, TEM images showed the long-range order of cylinder nanostructures [Figure 6n,m,l, respectively], as confirmed through SAXS analyses [Figure 6f,e,d, respectively] with peak ratios of $1:\sqrt{3}:\sqrt{4}$, where the PS volume fraction was in the range 0.3–0.38, consistent with previous findings for PVPh-*b*-PS/P4VP blends in which the PS volume fraction was in the range 0.28–0.41 for the cylinder structures.[15] Further increasing PMMA-*b*-P4VP concentrations to 50 and 60 wt % resulted in spherical micelle structures being observed in the TEM images [Figure 6k,j], as confirmed by only a single broad peak in the corresponding SAXS patterns [Figure 6c,b]. The

DOI: 10.1021/acs.macromol.9b01829
Macromolecules 2019, 52, 8374–8383

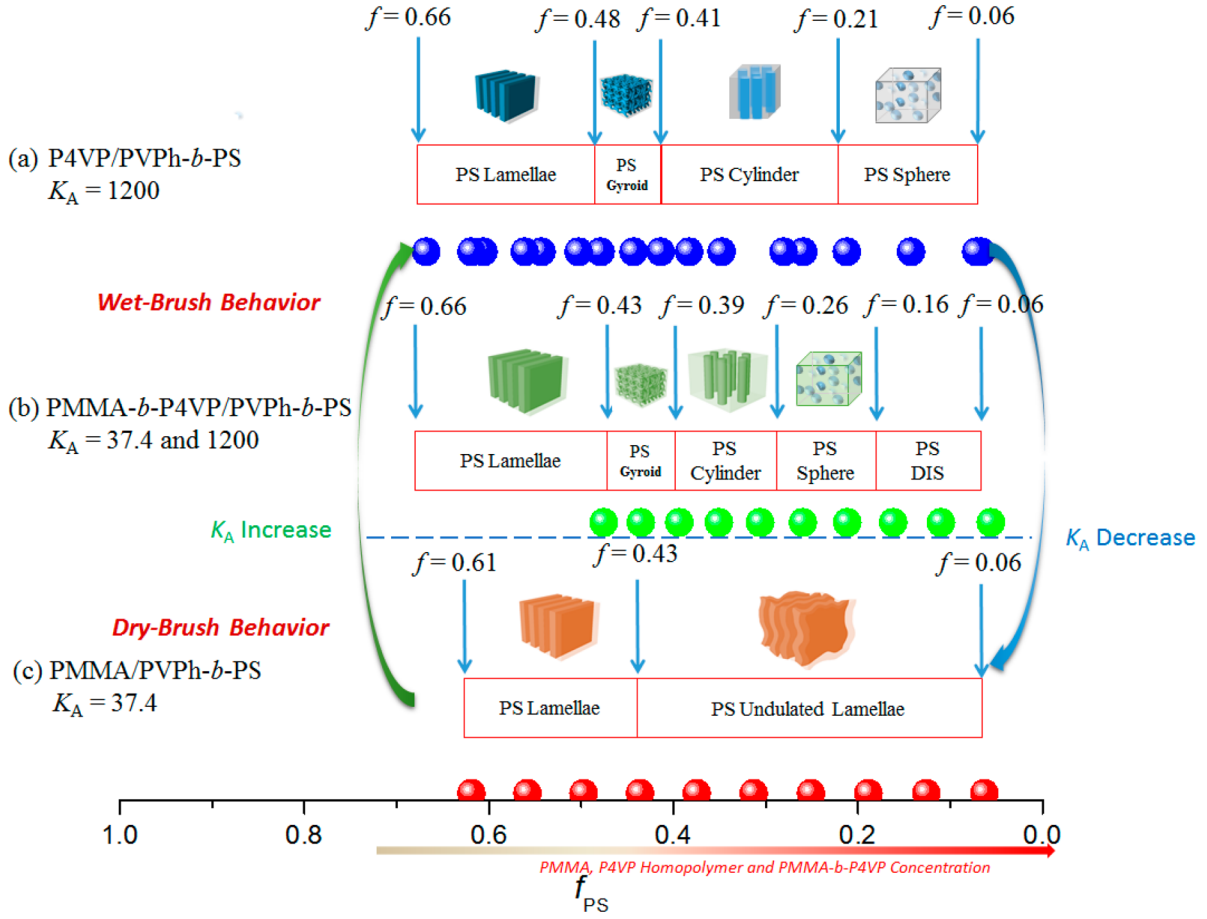

Figure 7. Phase diagram and volume fractions for PS block segment of (a) P4VP/PVPh-*b*-PS, (b) PMMA-*b*-P4VP/PVPh-*b*-PS, and (c) PMMA/PVPh-*b*-PS.

SAXS patterns featured no obvious or broad peaks upon increasing the P4VP-*b*-PMMA concentrations to 70−90 wt % [Figures S4a−c], suggesting disordered and short-range ordered micelle structures. This phenomenon is quite different in comparison of PVPh-*b*-PS/P4VP blend system, in which complete wet-brush behavior was observed with strong hydrogen bonding, as displayed in Figure 7a, and from the PVPh-*b*-PS/PMMA blend system, which exhibited only dry-brush or disordered structures with weak hydrogen bonding, as displayed in Figure 7c.[16] Combining P4VP and PMMA as block copolymer segments, this system displayed a full morphological transition from lamellae to double-gyroid, cylinder, sphere, and, finally, to disordered structures upon the addition of PMMA-*b*-P4VP into the PVPh-*b*-PS, as shown in Figure 7b. This result is novel because we observed all of the self-assembled nanostructures as well as a disordered structure, a finding that has never been reported previously. For example, even when decreasing the value of K_A by introducing P4VP into the PMMA segment, providing hydrogen bonding strength similar to that of the P2VP homopolymer, the double-gyroid structure was not found for the P2VP/PVPh-*b*-PS blend system.[16]

We also used FTIR spectroscopy to examine the intermolecular hydrogen bonding for the PMMA-*b*-P4VP/PVPh-*b*-PS mixtures (Figure 8). The area fraction of hydrogen-bonded P4VP pyridyl units was increased upon increasing the PVPh-*b*-PS concentrations [Figure 8B], but it was lower than PMMA-*b*-P4VP/PVPh system in Figure 4. This result is

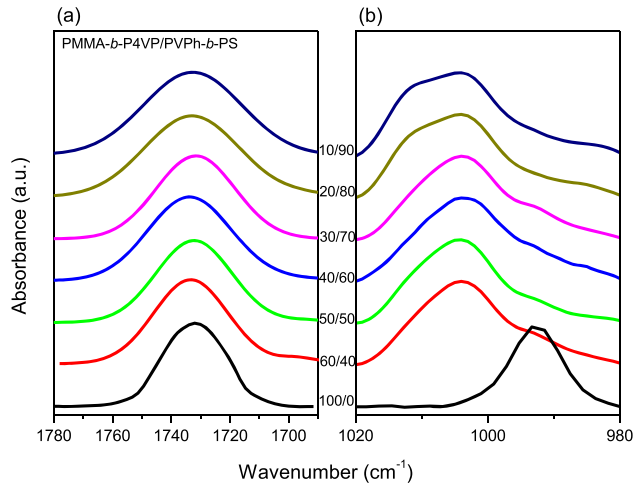

Figure 8. FTIR spectral analyses for PMMA-*b*-P4VP/PVPh-*b*-PS blends: (a) C═O groups and (b) pyridyl units.

reasonable because the PVPh volume fraction would decrease after covalent bonding with the PS block segment and because the area fraction of the pyridyl units did not reach 100%. As a result, we could not detect signals for any hydrogen-bonded PMMA C═O groups in Figure 8A or in Figure 4 for PMMA-*b*-P4VP/PVPh-*b*-PS mixtures. Based on this result, we conclude that the PVPh OH groups interacted only with P4VP, and not with PMMA, and, thus, we observed three-

DOI: 10.1021/acs.macromol.9b01829
Macromolecules 2019, 52, 8374−8383

phase behavior with only PS, PVPh/P4VP, and PMMA domains. However, the SAXS data in Figure 6 suggest that the scattering patterns were complicated for the PMMA-*b*-P4VP/PVPh-*b*-PS mixtures: the electron density difference (Table 1) among the two phases also featured six electron density differences, and thus, some q reflections might not have been clear, also probably because of the possible hierarchal nanostructures observed in this study.

For clarity, we further stained the diblock copolymer mixtures with RuO_4 for TEM imaging. P4VP block domains were revealed after staining with I_2 in TEM images, and PVPh and PMMA block domains were revealed after further staining with RuO_4; thus, PS block domain would appear white in PMMA-*b*-P4VP/PVPh-*b*-PS blends. For this study, we selected three compositions among the highly ordered self-assembled nanostructures observed through the SAXS and TEM analyses in Figure 6. Figure 9 displays TEM images for PMMA-*b*-P4VP/PVPh-*b*-PS = 30/70 stained with I_2 and with both I_2 and RuO_4. We observed only the cylinder structure when stained with I_2 [Figure 9a], whereas core−shell cylindrical structures appeared when stained with both I_2 and RuO_4 [Figure 9b,c] at this composition. The miscible PVPh/P4VP domains appeared dark because of hydrogen bonding; PS domains appeared white and the PMMA domain appeared gray [Figure 9d−f].

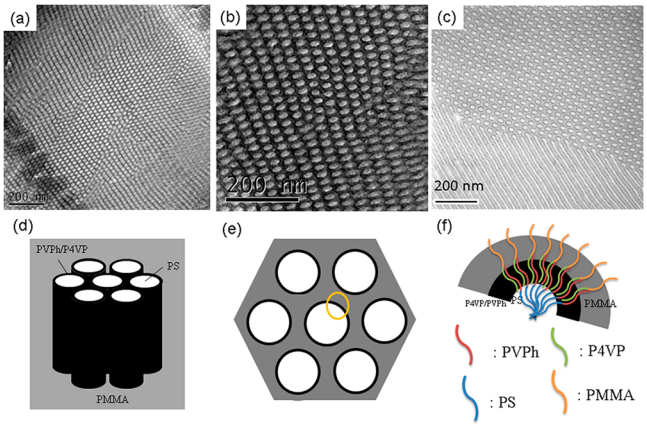

Figure 9. (a−c) TEM images for PMMA-*b*-P4VP/PVPh-*b*-PS = 30/70. (d−f) Schematic representation of the possible core/shell cylindrical structure, where the PMMA domain appears gray, PVPh/P4VP domain appears dark, and PS domain appears white.

Figure 10 presents TEM images of PMMA-*b*-P4VP/PVPh-*b*-PS = 20/80 stained with I_2, RuO_4, and stained with both I_2 and RuO_4. We observed only the closed cylinder structure when stained with I_2 [Figure 10a]; the equilibrium microphase separation of this closed cylinder structure was due to the intermaterial dividing surface (IMDS)[47]—the surface of constant mean curvature between the two microdomains. Because of the high value of T_g of the miscible PVPh/P4VP domain, the block chain conformation and corona thickness were compressed, becoming smaller than the corona block in terms of its unperturbed root-mean-square end-to-end distance. In addition, the lamellar and layer structure and a combination with a fuzzy cylinder structure appeared when stained only with RuO_4 [Figure 10b]. In Figure 10c, for the sample stained with both I_2 and RuO_4, the PS segment appeared in the white region (i.e., without staining I_2 and RuO_4) for the central cylindrical core of closed hexagonally packed structures. Surrounding the PS cylindrical core, we observed the shell of a miscible PVPh/P4VP domain, which appeared dark as a result of staining of the P4VP block with I_2. The corona of the miscible PVPh/P4VP domain shell, which arose from the PMMA domain, had the shape of hexagonal packing, and appeared as a result of staining with RuO_4. Similar to Figure 9d,e, the miscible PVPh/P4VP complex domain appeared dark; the PS domain appeared white and the PMMA domain gray, as displayed in Figure 10d,e. Finally, Figure 11 presents TEM images for PMMA-*b*-P4VP/PVPh-*b*-PS = 10/90 stained with both I_2 and RuO_4. The TEM images in Figure 11a,b reveal the long-range order of a core/shell double-gyroid structure from the [211] direction; the possible structures are summarized schematically in Figure 11c,d, similar to those in Figures 9 and 10.

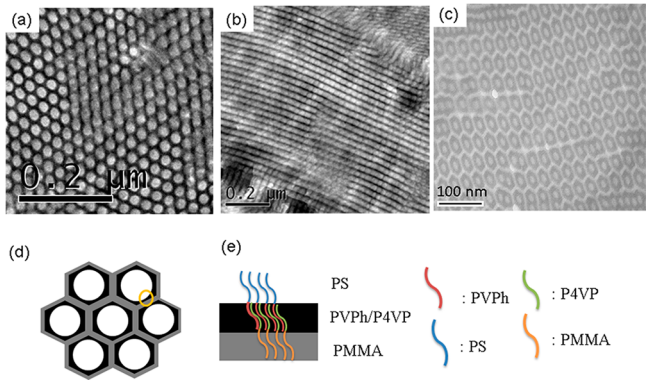

Figure 10. (a−c) TEM images for PMMA-*b*-P4VP/PVPh-*b*-PS = 20/80. (d, e) Schematic representation of the closed cylinder structure within the lamellae structure, where the PMMA domain appears gray, PVPh/P4VP domain appears dark, and the PS domain appears white.

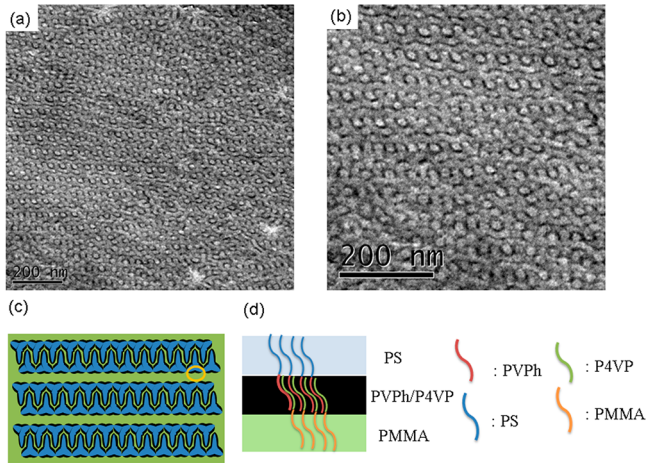

Figure 11. (a, b) TEM images for PMMA-*b*-P4VP/PVPh-*b*-PS = 10/90. (c, d) Schematic representation of the core/shell double-gyroid structure, where the PMMA domain appears green, the PVPh/P4VP domain appears dark, and the PS domain appears blue.

CONCLUSIONS

We have prepared PMMA-*b*-P4VP and PVPh-*b*-PS block copolymers by sequential anionic living polymerization. In PMMA-*b*-P4VP/PVPh blend system, the PVPh could act as the common solvent for PMMA-*b*-P4VP because the OH groups are able to interact with both pyridyl units and C═O

DOI: 10.1021/acs.macromol.9b01829
Macromolecules 2019, 52, 8374−8383

groups through hydrogen bonding and, thus, the self-assembled structures were observed to proceed from a cylinder structure to the short-range order of wormlike or micelle structures and, finally, to a miscible disordered structure. In addition, a full morphological transition—from lamellae to double-gyroid, cylinder, sphere, and, finally, disordered structures—occurred upon blending immiscible PMMA-*b*-P4VP into the PVPh-*b*-PS. Considering the ΔK effect, based on the different hydrogen bonding strengths between the PVPh/P4VP and PVPh/PMMA binary pairs, this AB/CD diblock copolymer mixture could form hierarchical self-assembled supramolecular structures, featuring PS, PVPh/PMMA, and PMMA domains, including core/shell cylinder, cylinder-in-lamellae, and core/shell double-gyroid structures.

■ ASSOCIATED CONTENT

Supporting Information

The Supporting Information is available free of charge on the ACS Publications website at DOI: 10.1021/acs.macromol.9b01829.

Interaction scheme, NMR, FTIR, and SAXS analyses of PMMA-*b*-P4VP and PVPh-*b*-PS diblock copolymer and their mixtures (PDF)

■ AUTHOR INFORMATION

Corresponding Author

*E-mail: kuosw@faculty.nsysu.edu.tw.

ORCID

Shiao-Wei Kuo: 0000-0002-4306-7171

Notes

The authors declare no competing financial interest.

■ ACKNOWLEDGMENTS

This study was supported financially by the Ministry of Science and Technology, Taiwan, under contracts MOST 108-2221-E-110-014-MY3 and 108-2638-E-002-003-MY2.

■ REFERENCES

(1) Guiod, A. R.; Vandermeulen, W. M.; Klok, V. H. Advanced drug delivery devices via self-assembly of amphiphilic block copolymers. *Adv. Drug Delivery Rev.* **2012**, *64*, 270−279.

(2) Lin, E. L.; Hsu, W. L.; Chiang, Y. W. Trapping structural coloration by a bioinspired gyroid microstructure in solid state. *ACS Nano* **2018**, *12*, 485−493.

(3) Tang, J.; Liu, J.; Li, C.; Li, Y.; Tade, M. O.; Dai, S.; Yamauchi, Y. Synthesis of nitrogen-doped mesoporous carbon spheres with extra-large pores through assembly of diblock copolymer micelles. *Angew. Chem., Int. Ed.* **2014**, *54*, 588−593.

(4) Cabral, H.; Miyata, K.; Osada, K.; Kataoka, K. Block Copolymer Micelles in Nanomedicine Applications. *Chem. Rev.* **2018**, *118*, 6844−6892.

(5) Yu, C. Y.; Kuo, S. W. Phenolic Functionality of Polyhedral Oligomeric Silsesquioxane Nanoparticles Affects Self-Assembly Supramolecular Structures of Block Copolymer Hybrid Complexes. *Ind. Eng. Chem. Res.* **2018**, *57*, 2546−2559.

(6) Yang, T.; Lei, Z.; Yang, S.; Chen, E. Q. Depletion driven self-assembly of block copolymer solutions by homopolymers. *Phys. Chem. Chem. Phys.* **2019**, *21*, 2121−2127.

(7) Qiu, H.; Oliver, A. M.; Gwyther, J.; Cai, J.; Harniman, R. L.; Hayward, D. W.; Manners, I. Uniform Toroidal Micelles via the Solution Self-Assembly of Block Copolymer−Homopolymer Blends Using a "Frustrated Crystallization" Approach. *Macromolecules* **2019**, *52*, 113−120.

(8) Doerk, G. S.; Li, R.; Fukuto, M.; Rodriguez, A.; Yager, K. G. Thickness-Dependent Ordering Kinetics in Cylindrical Block Copolymer/Homopolymer Ternary Blends. *Macromolecules* **2018**, *51*, 10259−10270.

(9) Montarnal, D.; Delbosc, N.; Chamignon, C.; Virolleaud, M. A.; Luo, Y.; Hawker, C. J.; Drockenmuller, E.; Bernard, J. Highly Ordered Nanoporous Films from Supramolecular Diblock Copolymers with Hydrogen-Bonding Junctions. *Angew. Chem., Int. Ed.* **2015**, *54*, 11117−11121.

(10) Chen, Y. W.; Yeh, B. J.; Hashimoto, T.; Liao, S. Y.; Lo, C. T. Hydrogen Bonding Induced Co-Ordering and Interfacial Curvature Controlled Crystallization Behavior of Binary Copolymer Blends. *Macromolecules* **2018**, *51*, 7699−7712.

(11) Zhao, J. Q.; Pearce, E. M.; Kwei, T. K. Binary and ternary blends of polystyrene-block-poly(p-hydroxystyrene). *Macromolecules* **1997**, *30*, 7119−7126.

(12) Kosoneen, H.; Ruokolainen, J.; Nyholm, P.; Ikkala, O. Self-organized cross-linked phenolic thermosets: thermal and dynamic mechanical properties of novolac/block copolymer blends. *Polymer* **2001**, *42*, 9481−9486.

(13) Dobrosielska, K.; Wakao, S.; Takano, A.; Matsushita, Y. Nanophase-separated structures of AB block copolymer/C homopolymer blends with complementary hydrogen-bonding interactions. *Macromolecules* **2008**, *41*, 7695−7698.

(14) Dobrosielska, K.; Wakao, S.; Suzuki, J.; Noda, K.; Takano, A.; Matsushita, Y. Effect of homopolymer molecular weight on nanophase-separated structures of AB block copolymer/C homopolymer blends with hydrogen-bonding interactions. *Macromolecules* **2009**, *42*, 7098−7102.

(15) Chen, S. C.; Kuo, S. W.; Jeng, U. S.; Su, C. J.; Chang, F. C. On modulating the phase behavior of block copolymer/homopolymer blends via hydrogen bonding. *Macromolecules* **2010**, *43*, 1083−1092.

(16) Tsai, S. C.; Lin, Y. C.; Lin, E. L.; Chiang, Y. W.; Kuo, S. W. Hydrogen bonding strength effect on self-assembly supramolecular structures of diblock copolymer/homopolymer blends. *Polym. Chem.* **2016**, *7*, 2395−2409.

(17) Dehghan, A.; Shi, A. C. Modeling hydrogen bonding in diblock copolymer/homopolymer blends. *Macromolecules* **2013**, *46*, 5796−5805.

(18) Hameed, N.; Guo, Q. Nanostructure and hydrogen bonding in interpolyelectrolyte complexes of poly(ε-caprolactone)-*block*-poly(2-vinyl pyridine) and poly(acrylic acid). *Polymer* **2008**, *49*, 5268−5275.

(19) Hameed, N.; Liu, J.; Guo, Q. Self-assembled complexes of poly(4-vinylphenol) and poly(ε-caprolactone)-block-poly(2-vinylpyridine) via competitive hydrogen bonding. *Macromolecules* **2008**, *41*, 7596−7605.

(20) Hameed, N.; Guo, Q. Selective hydrogen bonding and hierarchical nanostructures in poly(hydroxyether of bisphenol A)/poly(ε-caprolactone)-*block*-poly(2-vinyl pyridine) blends. *Polymer* **2008**, *49*, 922−933.

(21) Chen, W. C.; Kuo, S. W.; Lu, C. H.; Jeng, U. S.; Chang, F. C. Self-assembly structures through competitive interactions of crystalline-amorphous diblock copolymer/homopolymer blends: Poly(ε;-caprolactone-b-4-vinylpyridine)/poly(vinyl phenol). *Macromolecules* **2009**, *42*, 3580−3590.

(22) Salim, N. V.; Hanley, T.; Guo, Q. Microphase separation through competitive hydrogen bonding in double crystalline diblock copolymer/homopolymer blends. *Macromolecules* **2010**, *43*, 7695−7704.

(23) Li, J. G.; Lin, Y. D.; Kuo, S. W. From microphase separation to self-organized mesoporous phenolic resin through competitive hydrogen bonding with double-crystalline diblock copolymers of poly(ethylene oxide-b-ε-caprolactone). *Macromolecules* **2011**, *44*, 9295−9309.

(24) Hameed, N.; Salim, N. V.; Guo, Q. Microphase separation through competitive hydrogen bonding in self-assembled diblock copolymer/homopolymer complexes. *J. Chem. Phys.* **2009**, *131*, 214905.

DOI: 10.1021/acs.macromol.9b01829
Macromolecules 2019, 52, 8374−8383

(25) Lee, H. F.; Kuo, S. W.; Huang, C. F.; Lu, J. S.; Chan, S. C.; Wang, C. F.; Chang, F. C. Hydrogen-bonding interactions mediate the phase behavior of an AB/C block copolymer/homopolymer blend comprising poly (methyl methacrylate-b-vinylpyrrolidone) and poly (vinylphenol). *Macromolecules* **2006**, *39*, 5458−5465.
(26) Chen, W. C.; Kuo, S. W.; Jeng, U. S.; Chang, F. C. Self-assembly through competitive interactions of miscible diblock copolymer/homopolymer blends: Poly (vinylphenol-b-methyl methacrylate)/poly (vinylpyrrolidone) blend. *Macromolecules* **2008**, *41*, 1401−1410.
(27) Zhou, J.; Shi, A. C. Microphase separation induced by differential interactions in diblock copolymer/homopolymer blends. *J. Chem. Phys.* **2009**, *130*, 234904.
(28) Lin, I.; Kuo, S. W.; Chang, F. C. Self-Assembly structures through competitive interactions of miscible crystalline−amorphous diblock copolymer/homopolymer blends. *Polymer* **2009**, *50*, 5276−5287.
(29) Lin, R. C.; Kuo, S. W. Hydrogen Bonding Interactions Mediated Self-assembly Structures of Multicomponent Block Copolymer Mixtures. *Acta Polym. Sin.* **2018**, *8*, 789−805.
(30) Auschra, C.; Stadler, R. New ordered morphologies in ABC triblock copolymers. *Macromolecules* **1993**, *26*, 2171−2174.
(31) Zheng, W.; Wang, Z. G. Morphology of ABC Triblock Copolymers. *Macromolecules* **1995**, *28*, 7215−7223.
(32) Matsushita, Y. Creation of hierarchically ordered nanophase structures in block polymers having various competing interactions. *Macromolecules* **2007**, *40*, 771−776.
(33) Miyase, H.; Asai, Y.; Takano, A.; Matsushita, Y. Kaleidoscopic tiling patterns with large unit cells from ABC star-shaped terpolymer/diblock copolymer blends with hydrogen bonding interaction. *Macromolecules* **2017**, *50*, 979−986.
(34) Asari, T.; Matsuo, S.; Takano, A.; Matsushita, Y. Three-phase hierarchical structures from AB/CD diblock copolymer blends with complemental hydrogen bonding interaction. *Macromolecules* **2005**, *38*, 8811−8815.
(35) Asari, T.; Arai, S.; Takano, A.; Matsushita, Y. Archimedean tiling structures from ABA/CD block copolymerblends having intermolecular association with hydrogen bonding. *Macromolecules* **2006**, *39*, 2232−2237.
(36) Kuo, S. W. Hydrogen bond-mediated self-assembly and supramolecular structures of diblock copolymer mixtures. *Polym. Int.* **2009**, *58*, 455−464.
(37) Chen, W. C.; Kuo, S. W.; Chang, F. C. Self-assembly of an A−B diblock copolymer blended with a C homopolymer and a C−D diblock copolymer through hydrogen bonding interaction. *Polymer* **2010**, *51*, 4176−4184.
(38) Tseng, T. C.; Kuo, S. W. Hydrogen-Bonding Strength Influences Hierarchical Self-Assembled Structures in Unusual Miscible/Immiscible Diblock Copolymer Blends. *Macromolecules* **2018**, *51*, 6451−6459.
(39) Tseng, T. C.; Kuo, S. W. Hierarchical Self-Assembled Structures from Diblock Copolymer Mixtures by Competitive Hydrogen Bonding Strength. *Molecules* **2018**, *23*, 2242.
(40) Tseng, T. C.; Kuo, S. W. Hydrogen bonding induces unusual self-assembled structures from mixtures of two miscible disordered diblock copolymers. *Eur. Polym. J.* **2019**, *116*, 361−369.
(41) Tung, P. H.; Kuo, S. W.; Chen, S. C.; Lin, C. L.; Chang, F. C. Micellar morphologies of self-associated diblock copolymers in acetone solution. *Polymer* **2007**, *48*, 3192−3200.
(42) Kuo, S. W.; Tung, P. H.; Lai, C. L.; Jeong, K. U.; Chang, F. C. Supramolecular micellization of diblock copolymer mixtures mediated by hydrogen bonding for the observation of separated coil and chain aggregation in common solvents. *Macromol. Rapid Commun.* **2008**, *29*, 229−233.
(43) Kuo, S. W.; Tung, P. H.; Chang, F. C. Hydrogen bond mediated supramolecular micellization of diblock copolymer mixture in common solvents. *Eur. Polym. J.* **2009**, *45*, 1924−1935.
(44) Kwei, T. K. The Effect of Hydrogen Bonding on the Glass Transition Temperatures of Polymer Mixtures. *J. Polym. Sci., Polym. Lett. Ed.* **1984**, *22*, 307−313.
(45) Kuo, S. W.; Tung, P. H.; Chang, F. C. Syntheses and the study of strongly hydrogen-bonded poly (vinylphenol-b-vinylpyridine) diblock copolymer through anionic polymerization. *Macromolecules* **2006**, *39*, 9388−9395.
(46) Kuo, S. W. *Hydrogen Bonding in Polymeric Materials*; John Wiley & Sons: Hoboken, NJ, 2018.
(47) Giod, S. P.; Schwark, D. W.; Thomsa, E. L.; Gonsalves, M. Observation of a Non-Constant Mean Curvature Interface in an ABC Triblock Copolymer. *Macromolecules* **1993**, *26*, 2636−2640.

DOI: 10.1021/acs.macromol.9b01829
Macromolecules 2019, 52, 8374−8383